NAG1-441

Semiannual Progress Report

Submitted to:	National Aeronautics and Space Adminstration Langley Research Center Hampton, Va 23665
Institution:	Hampton University Dept of Physics and Engineering
Title of Research:	Direct Solar-Pumped Iodine Laser Amplifier
NASA Grant Number	NAG-1-441
Period Covered	April 1, 1985 - Sept 30, 1985
Principal Investigator	Dr. Kwang S. Han

Direct Solar-Pumped Iodine Laser Amplifier

Contents

I. Introduction 1

II. Progress in experiments of the iodine laser amplifier pumped by Vortek solar simulator. 1

III. Progress in kinetic modeling of the solar pumped iodine laser 5

IV. Progress in parmaetric studies of dye laser amplifier by Tamarack solar simulator 6

Figures 9

Appendix 21

I. Introduction

This semiannual progress report covers the period from April 1, 1985 to Sept 30, 1985 under NASA grant NAG-1-441 entitled "Direct solar-pumped iodine laser amplifier". During this period the parametric studies of the iodine laser oscillator pumped by a Vortek simulator has been carried out before amplifier studies. The amplifier studies are postponed to the extended period after completing the parametric studies. In addition, the kinetic modeling of a solar-pumped iodine laser amplifier, and the experimental work for a solar pumped dye laser amplifier are in progress. This report contains three parts: (1) the radiation characteristics of solar simulator and the parametric characteristics of photodissociation iodine laser continously pumped by a Vortek solar simulator, (2) kinetic modeling of a solar-pumped iodine laser amplifier, and (3) the study of the dye laser amplifier pumped by a Tamarack solar simulator.

II. Progress in experiments of the iodine laser amplifier pumped by Vortek solar simulator.

Direct solar pumped iodine laser experiment has been done in two directions: (a) Determination of radiation characteristics of the Vortek solar simulator and (b) operation of a continuously pumped iodine laser oscillator.

(a) Determination of radiation characteristics of the Vortek solar simulator.

In this experiment the Vortek arc lamp is used as a pumping source of the photodissociation iodine laser. Therefore the determination of radiation characteristic of the lamp is needed. The optical radiation is produced in the lamp by a high pressure dc argon arc, which is vortex stabilized and deionized water cooled. The arc is contained in a single quartz (Germasil grade) tube of

2.1 cm diameter and 25 cm long with replaceable water - cooled tungsten electrodes at each end. Rapidly swirling water inside of this tube efficiently removes the excess heat and prevents deposition of electrode material. The arc size is 1.1 cm diameter and 15 cm long and its emission is in the spectral range of 200 nm to 1400 nm. In order to measure the spectral irradiance, a deuterium irradiance standard lamp (Optronics model 45) is used to calibrate the spectrometer and the detector. In measurements wherein two sources (standard source and Vortek arc lamp) are being compared by the direct substitution method (slit widths kept unchanged, use of the same detector), thus neither knowledge of the spectral transmittance of the spectrometer, nor knowledge of the spectral sensitivity of the detector is required. The linearity of the response of the detector is predetermined because the detector response for the standard source is significantly below that of the Vortek arc lamp. The spectral irradiance of Vortek arc lamp is measured at a distance 120" to avoid the effect of the difference of the two sources a geometrical shape. The measured spectral irradiance for various currents are shown in table 1. These values are plotted in Fig. 1 which shows the spectral irradiance curve of the Vortek arc lamp in the range of 200nm to 400 nm. The peak irradiance is 70 uw/cm^2.nm at a wavelength 350 nm. In order to compare with the AM0 (air mass zero) solar radiation, two irradiances are normalized at a wavelength 300 nm where two irradiances are very similiar. As shown in figure 2, the Vortek arc lamp produces more UV radiation in the absorption band of C_3F_7I than the solar radiation. The irradiance of the arc lamp at 270nm (absorption peak of C_3F_7I) is plotted as function of the current in fiugre 3. The irradiance is proportional to the square of current of the arc lamp, indicating that the resistance of the plasma generated by the arc lamp is constant.

(b) Operation of a continuously pumped iodine laser.

Figure 4 shows the schematics of the experimental setup for cw iodine laser pumping by the Vortek solar simulator. The laser tube and the arc lamp, which is coupled by an elliptical and cylindrical reflector, are located at each of the focal lines. The laser tube is made of a suprasil quartz tube with a 12 mm inner diameter and is surrounded by water cooling jacket. The iodide flowing system consists of two reserviors; one for vaporization and the other for condensation. In order to prevent the temperature variation by vaporization, the vaporization reservoirw as kept at room temperature. The condensation reservior was kept on the liquid nitrogen temperature. The flow rate, which is controlled by an adjustable valve, is measured by using mass flowmeter (Hasting Co., model AHL-2G) calibrated for C_3F_7I. To calculate the velocity of iodide molecules in the laser tube, the inlet and the outlet pressures are measured.

Fig. 5 through 7 show the laser signals versus time obtained by using the Ge detector. Laser excitaiton was continuously obserserved for over one hour without any break. Fig. 6 shows the periodic variation of the laser signal due to the ripple of the input power of the solar simulator. Fig. 7 shows more details of the spike pulses appeared in figure 6 and shows the dc offset of the spikes. Laser output power is measured as function of various flow rates of the iodides for two different currents of arc lamp as shown in figure 8. The maximum output power, 1.3W, is obtained at the flow rate of 1740 sccm, which is equivalent to a velocity of 18 m/s for both currents.

Finally, laser output power is measured for the various transmissions of output coupler mirrors to optimize the laser cavity condition. In this measurement the current of arc lamp and the flow rate of iodides are kept

constant. As shown in figure 9, an optimum cavity condition is obtained at 15% transmission of the output coupler mirror for power output of 1.3 Watts. In addition, research is under way to find the optimum condition for laser tube of different cross sections and currents. The results will be reported in the next progress report.

III. Progress in kinetic modeling of the solar-pumped iodine laser

A kinetic model for a solar simulator pumped iodine laser system is being developed and compared to an experiment in which the solar simulator output is dispersed over a large active volume (150 cm^3) with low simulator light intensity (= 200 solar constants). A trace foreign gas which quenches the upper level is introduced into the model. Furthermore, a constant representing optical absorption of the simulator emission is introduced, in addition to a constant representing the scattering at each of the mirrors, via the optical cavity time constant. The non-uniform heating of the gas is treated as well as the pressure change as a function of time within the cavity. With these new phenomena introduced into the kinetic model, a best reasonable fit to the experimental data is found by adjusting the reaction rate coefficients within the range of known uncertainity by numerical methods. The experimental parameters modeled are the lasing time, laser pulse energy, and the laser threshold. See details in Appendix. (NASA Technical Paper L)

IV. Progress in parametric studies of dye laser amplifier pumped by Tamarack solar simulator

Most of research effort about the amplification characteristics of dye laser are directed to the strongly pumped laser amplifier (more than $2.5x10^4 W/cm^2$). In contrast to the conventional dye laser amplifier, the solar-pumped dye laser amplifier is limited by the geometrical factor of solar concentration ($4x10^4$ solar constant). Consequently the strongly pumped laser is not possible. Therefor both our experimental and theoretical work is directed to evaluate the feasibility of developing a solar-simulator pumped dye laser amplifier. The pumping source for dye laser amplifier is the Tamarack simulator at Langley Research Center. The Tamarack simulator generates light from electrical arc between electrodes (gap=8mm) stabilized by a continous flow of xenon gas (fill pressure=1,030KPa or 1.02atm). The output power of Tamarack solar simulator is 4kW with an electrical input of 40kW. In order to gain maximum output from the dye laser amplifier, investigation of dye parmaeters such as flow rate of dye solution, dye concentration, quenching factor and coupling between solar simulator and laser amplifier system is neccessary to evaluate the solar radiation pumped amplifier system in space. Our study have been centered around the design of dye cell which allows transverse flowing with a flow rate of 4 gal/min in order to pass through the amplifier cell within 500us which is the life time of rhodamine 6G dye. It has been noted that the further modification of the newly designed dye cell is necessary for the dye laser amplifier to be coupled efficiently with the solar simulator. Figure 10 shows schematic diagram of experimental setup for the continuously solar-pumped dye laser amplifier. Figure 11 shows schematic

diagram of a newly-designed dye cell. Figure 12 shows dye oscillator output as function of input power. The result indiactes that oscillator output linearly increses with the input power.

Table 1. Spectral irradiance ($\mu W/cm^2 \cdot nm$) of Vortek simulator at a distance 120".

Wavelength(nm)	Current (A)								
	120	140	160	180	200	220	240	260	280
200	.076	.095	.114	.133	.152	.189	.208	.246	.303
210	.074	.089	.101	.119	.137	.160	.190	.221	.267
220	.128	.147	.186	.217	.267	.300	.342	.412	.476
230	1.05	1.28	1.41	1.74	2.27	2.73	3.00	3.65	4.16
240	3.59	3.97	4.92	6.18	7.73	8.77	10.3	12.9	15.2
250	4.60	5.83	7.44	9.43	11.8	13.8	16.5	20.7	25.2
260	5.52	7.12	9.19	11.5	14.6	17.2	20.7	25.9	31.3
270	6.25	8.06	10.6	13.3	16.6	19.7	23.2	29.5	35.5
280	6.98	9.17	11.8	15.0	18.3	22.3	26.5	33.6	40.9
290	7.83	9.88	13.1	16.1	20.2	23.7	29.5	36.1	44.6
300	8.31	10.8	13.8	17.7	22.0	25.9	32.0	40.3	48.2
310	8.90	11.6	15.1	19.0	24.1	28.6	34.4	42.7	53.1
320	9.62	12.7	16.4	21.3	26.2	31.7	38.1	48.4	58.8
330	10.3	13.1	17.1	21.9	27.9	33.0	40.7	50.9	62.0
340	11.5	14.7	19.4	25.0	31.2	37.6	46.1	57.0	68.3
350	11.1	13.4	19.2	24.3	30.9	37.0	45.0	56.6	68.7
360	11.3	14.8	18.7	24.8	31.2	37.8	46.0	59.1	68.4
370	11.0	14.3	17.8	23.9	29.8	35.6	44.8	55.1	65.3
380	10.7	13.8	17.1	22.9	29.2	35.3	43.6	53.9	63.4
390	10.5	13.7	16.2	22.3	29.0	35.3	43.0	52.9	61.2
400	9.92	12.6	15.4	20.7	26.4	31.9	39.3	48.8	57.4

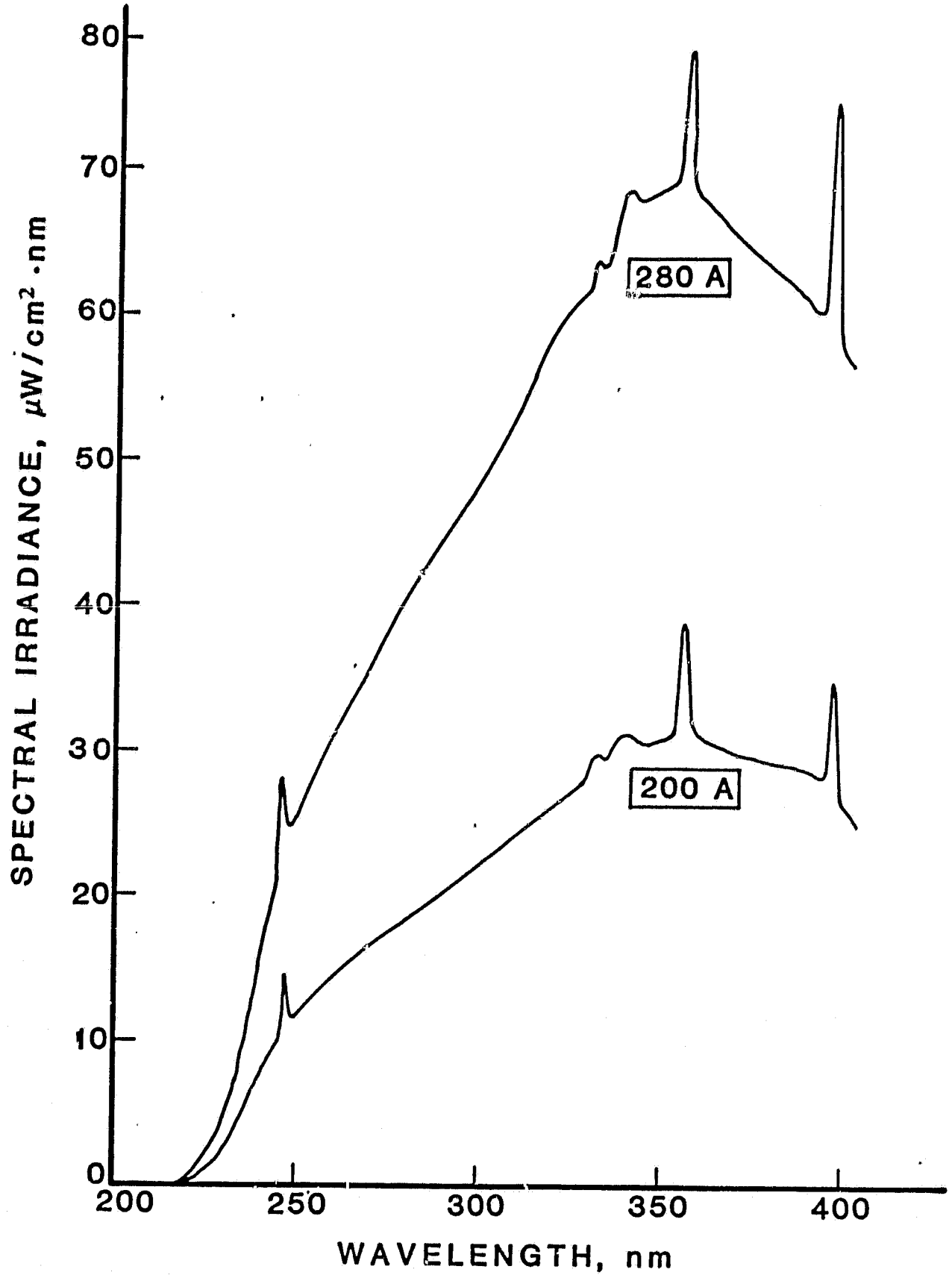

Fig. 1 Spectral irradiance curve of Vortek arc lamp at a distance of 120 inches.

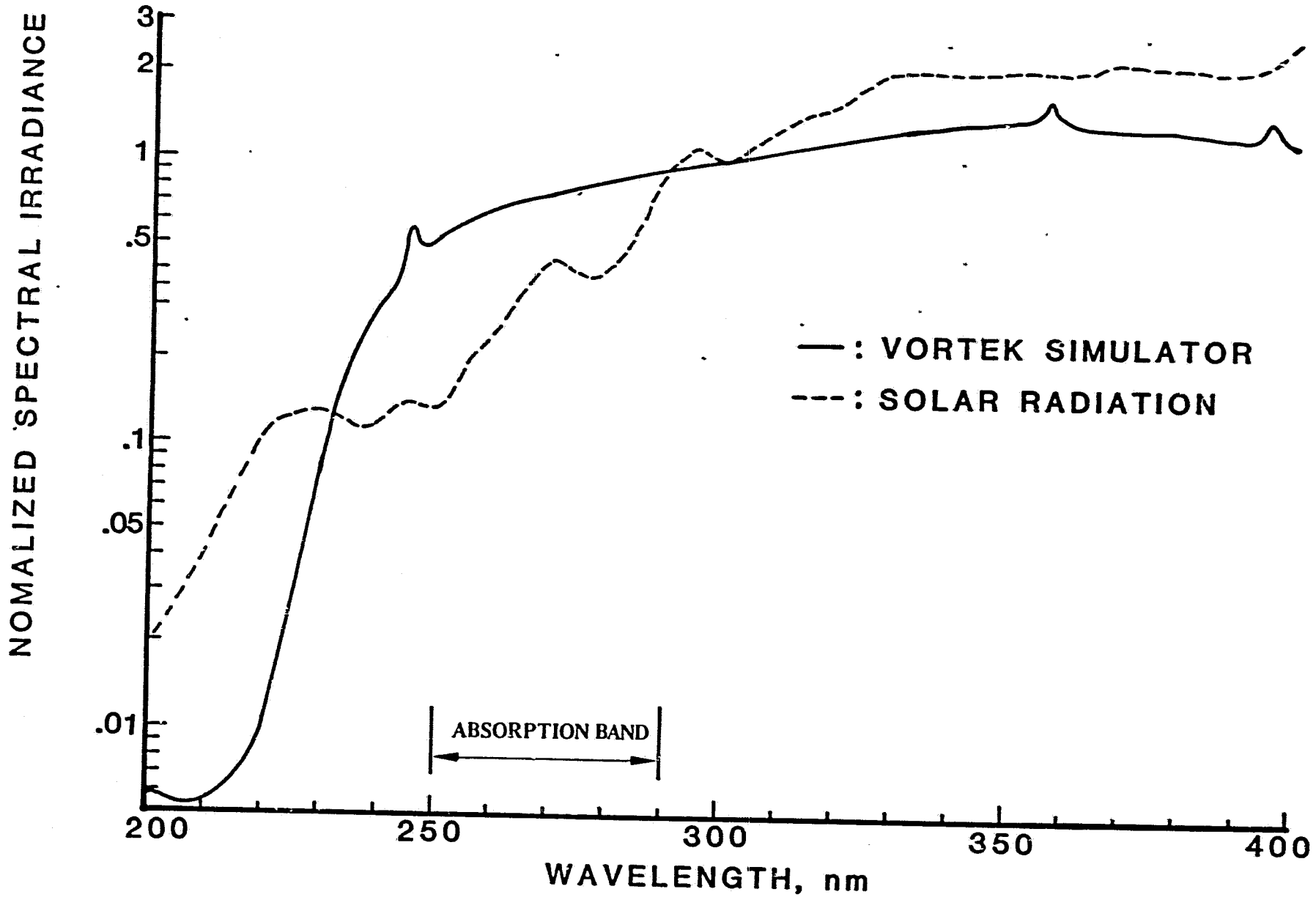

Fig. 2. Normalized spectral irradinance of Vortek arc lamp at 300nm.

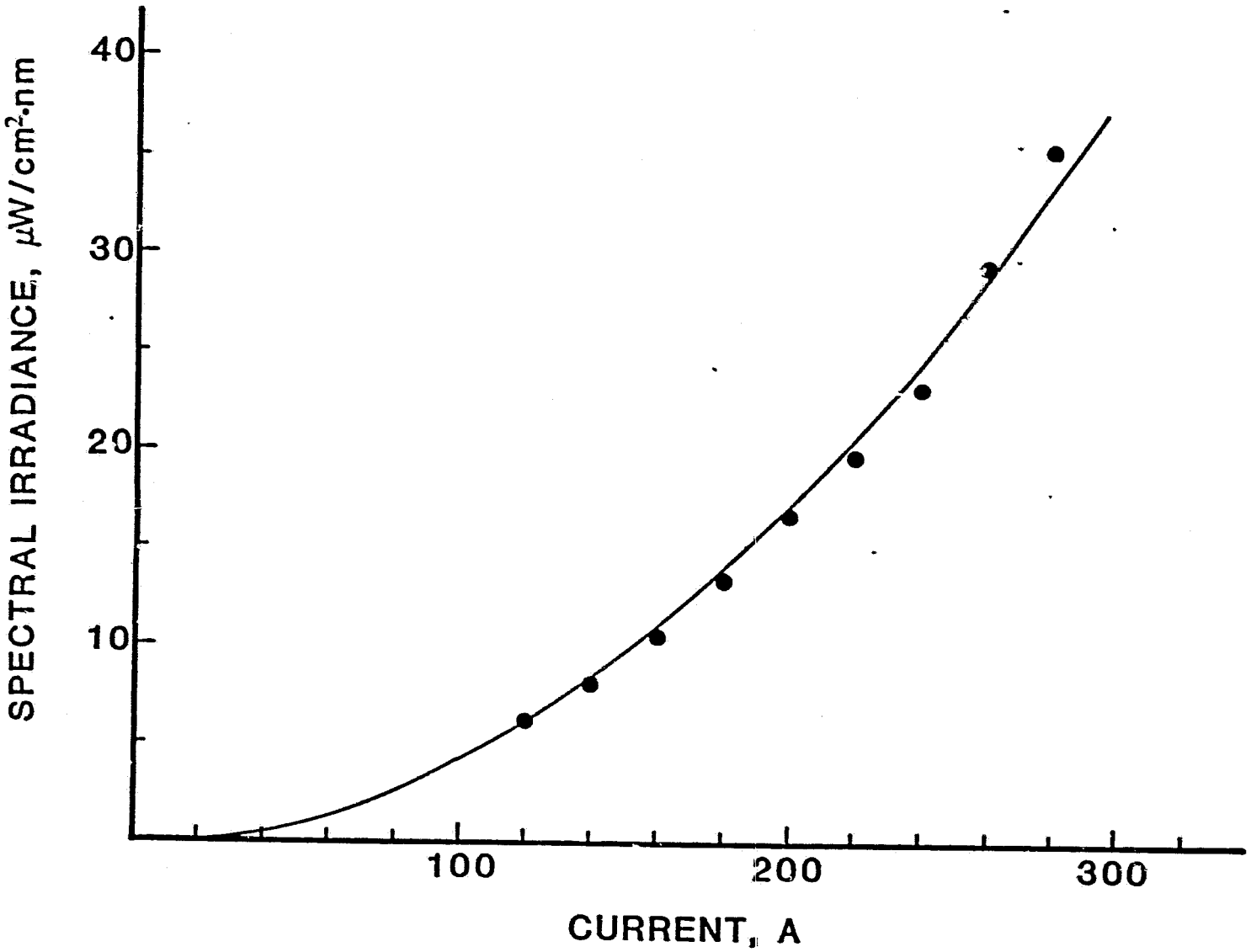

Fig. 3. The irradiance of the arc lamp at 270nm (absorption peak o C_3F_7I) as function of current.

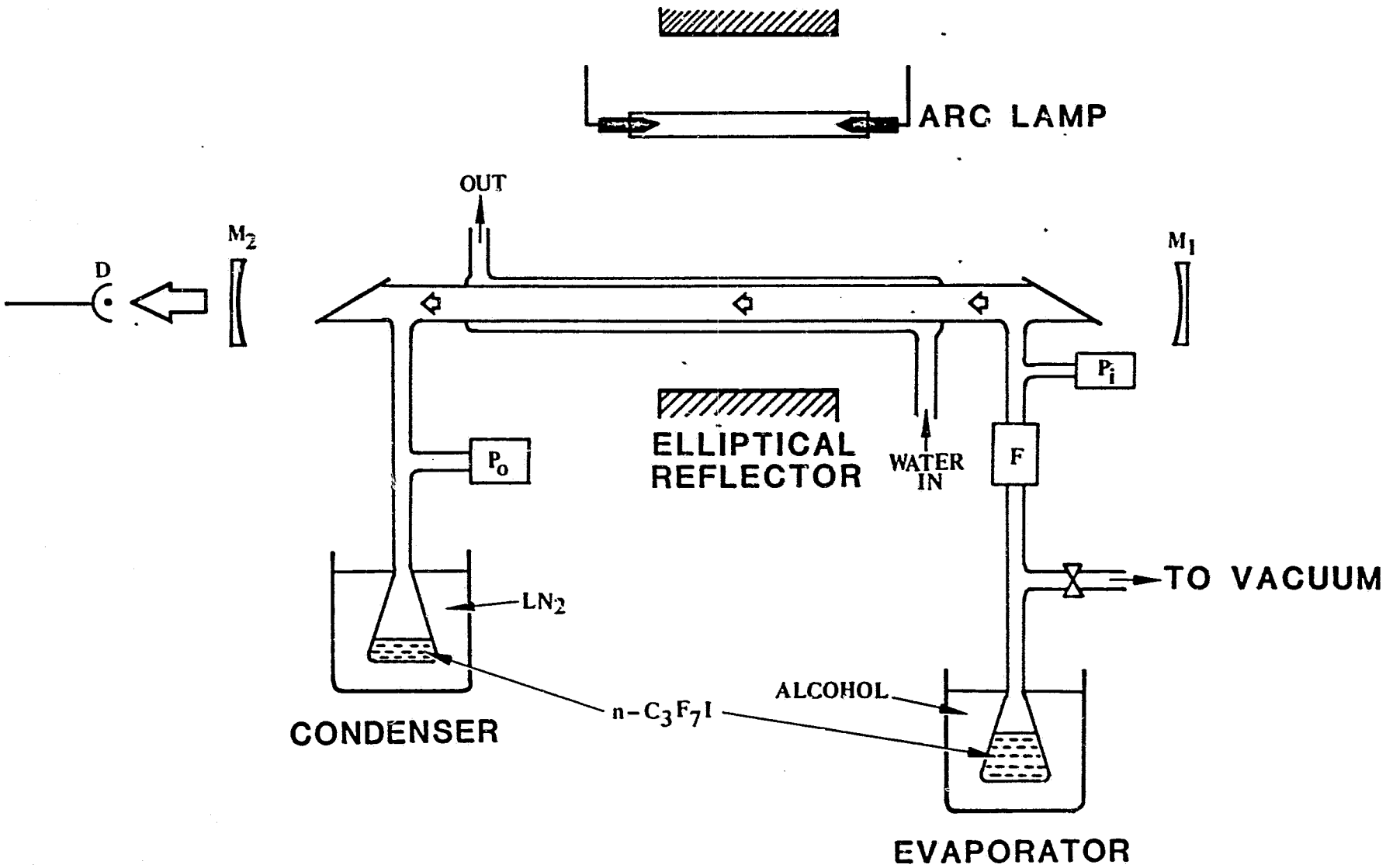

Fig. 4. The schematics of experimental setup for CW idoine laser pumping by Vortek solar simulator.

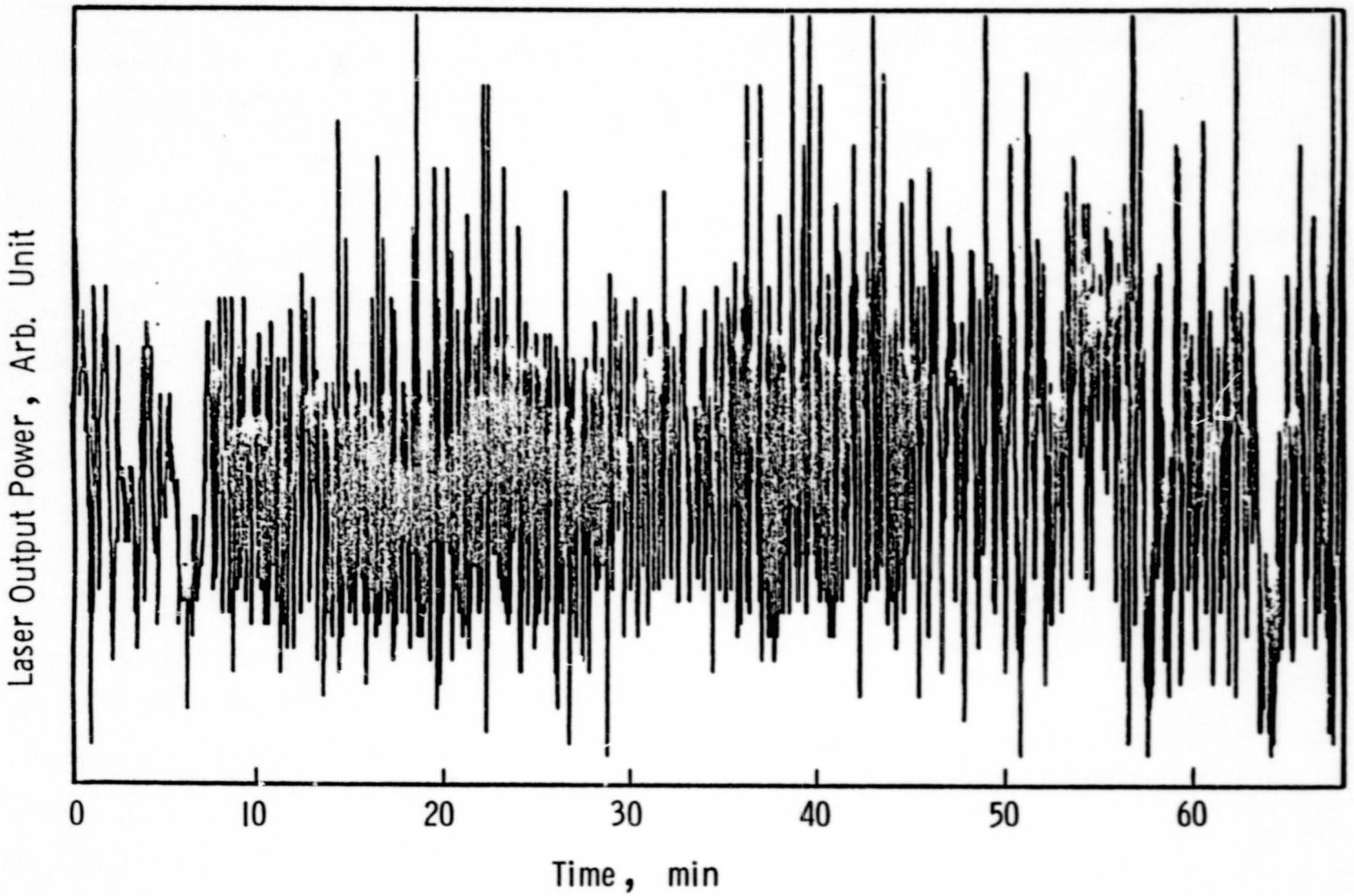

Fig. 5. The laser signal as a functio[illegible]f time.

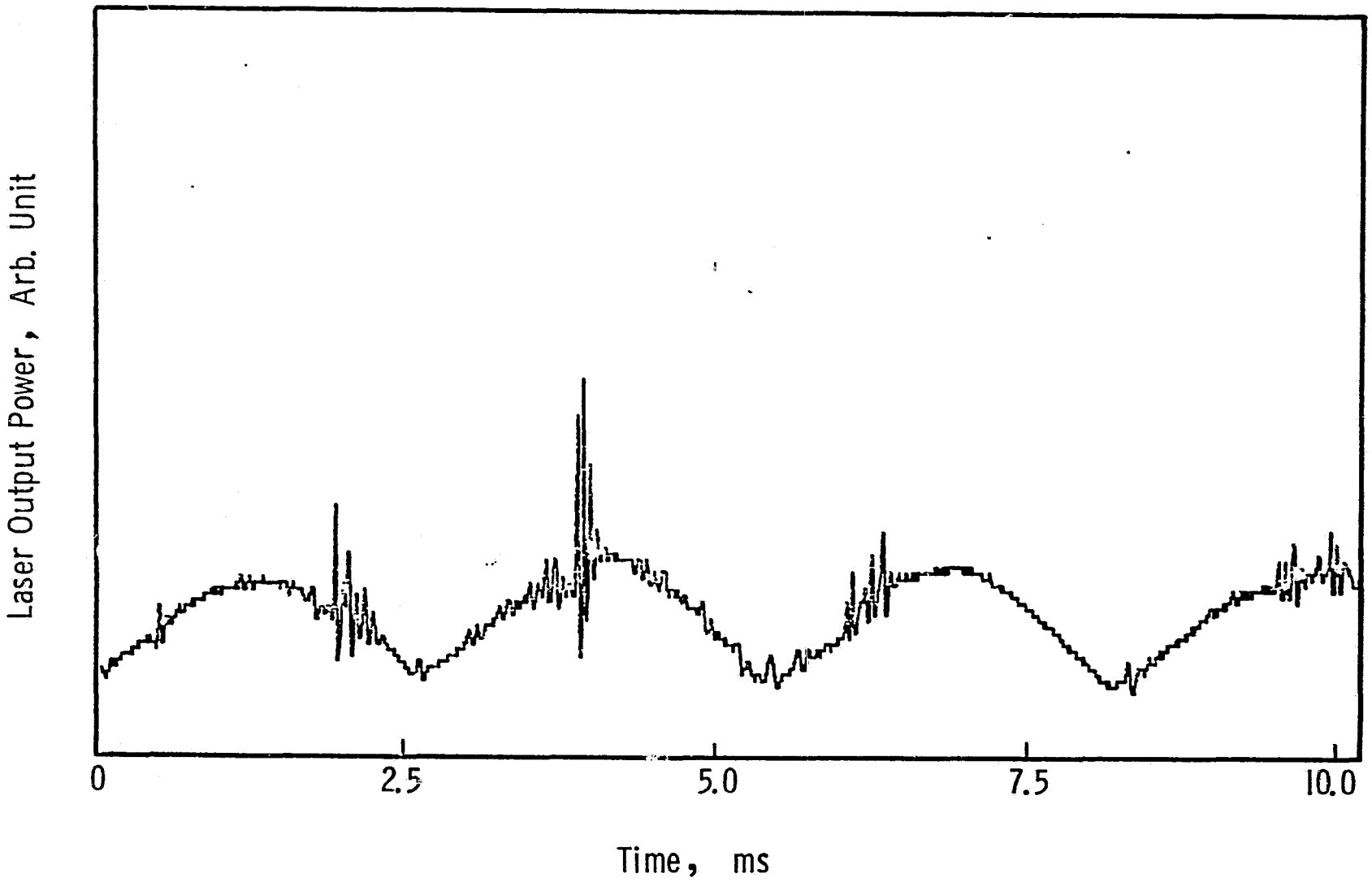

Fig. 6. Laser signal as a function of time.

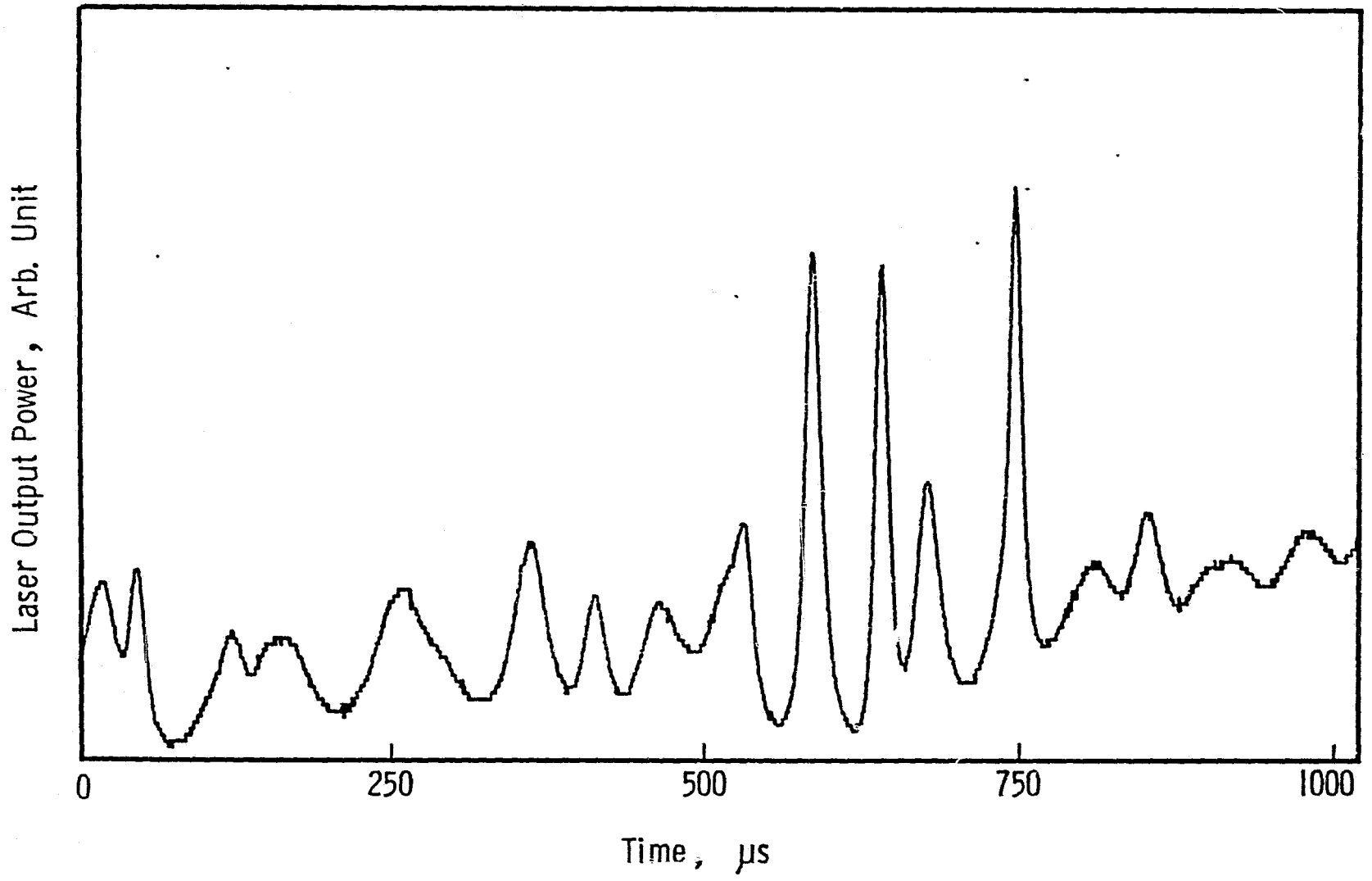

Fig. 7. Laser signal as a function of time.

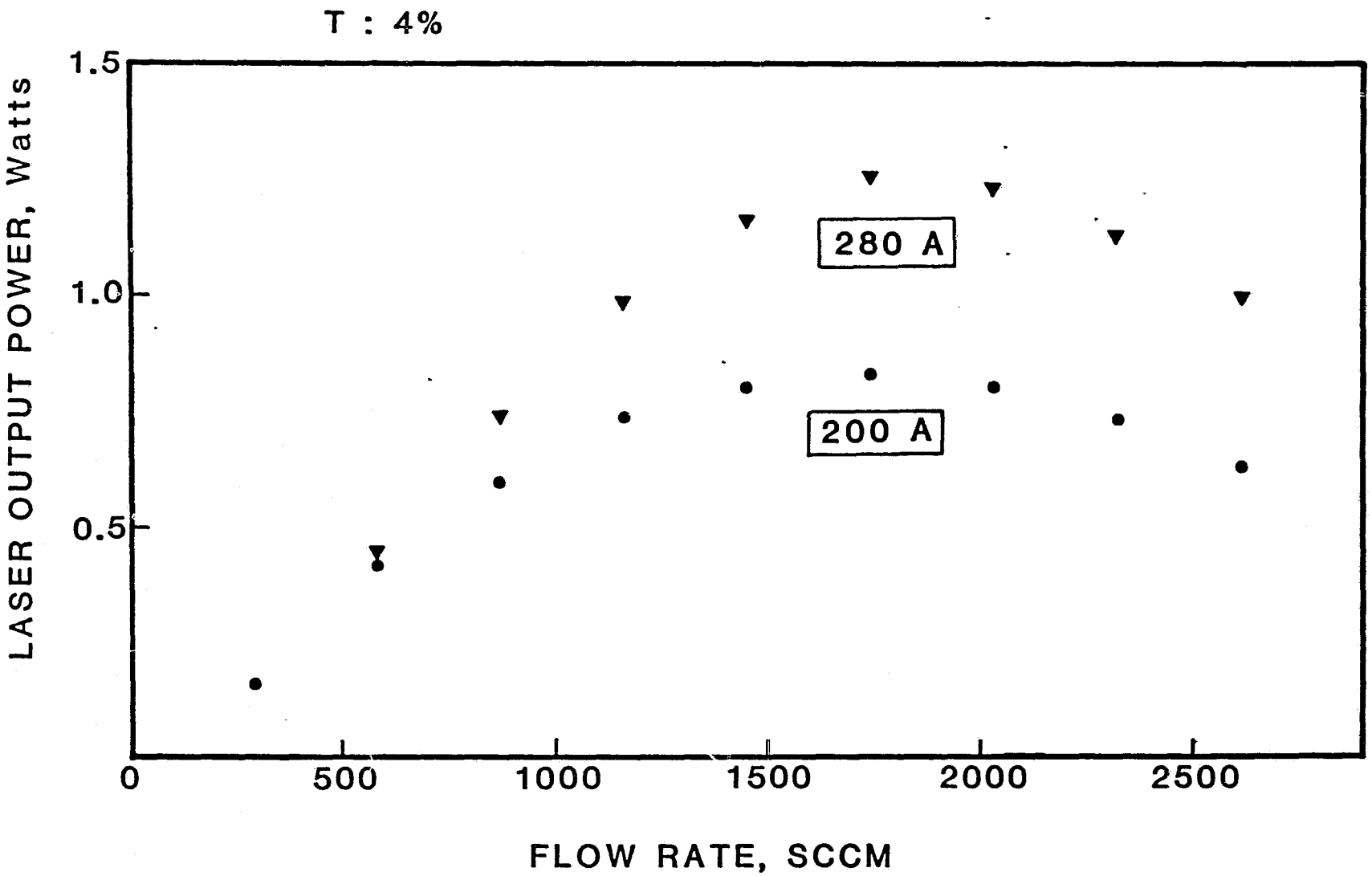

Fig. 8. Laser signal as a function of time.

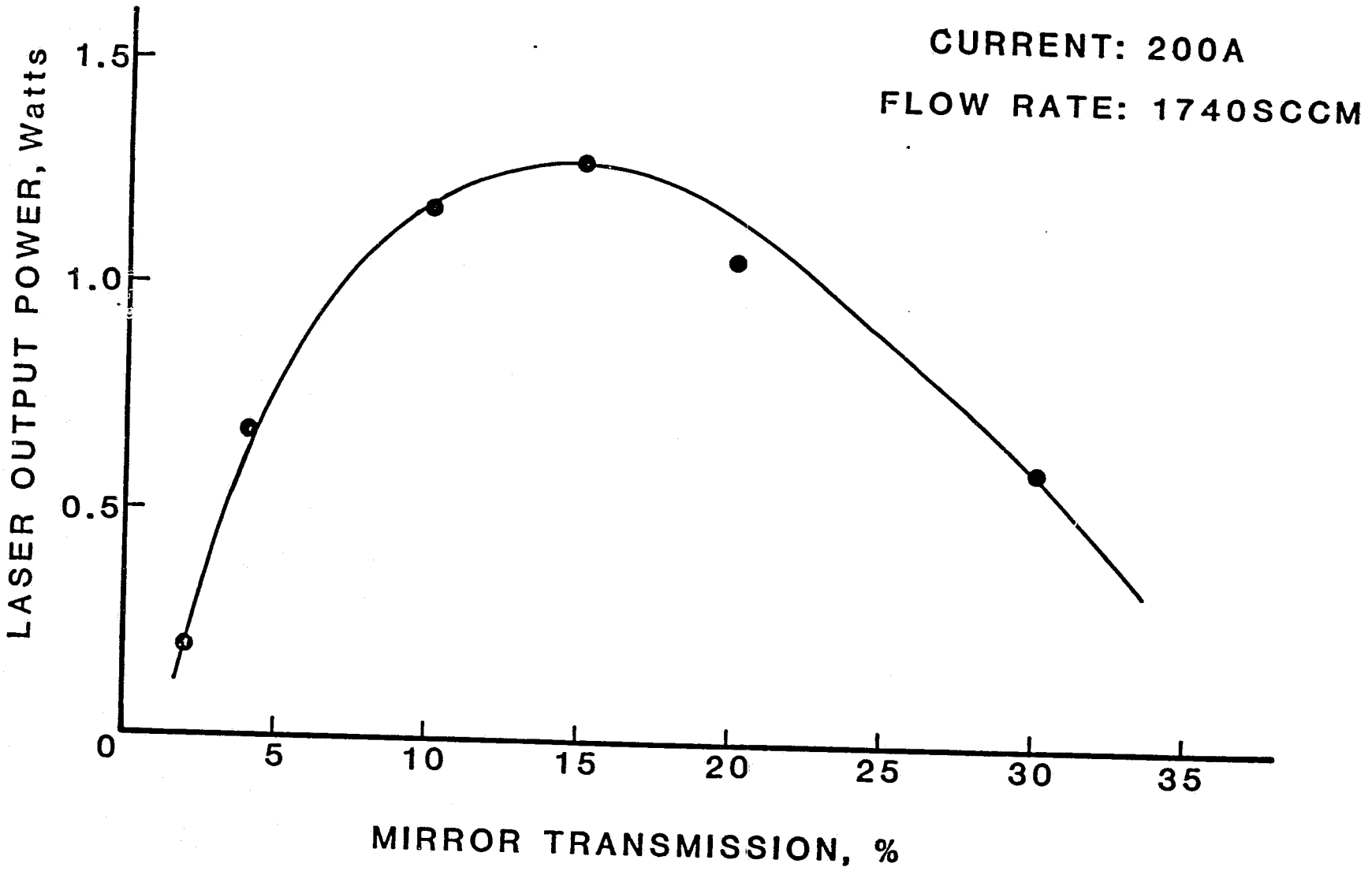

Fig. 9. Laser output power as a function of transmission of output coupler mirror.

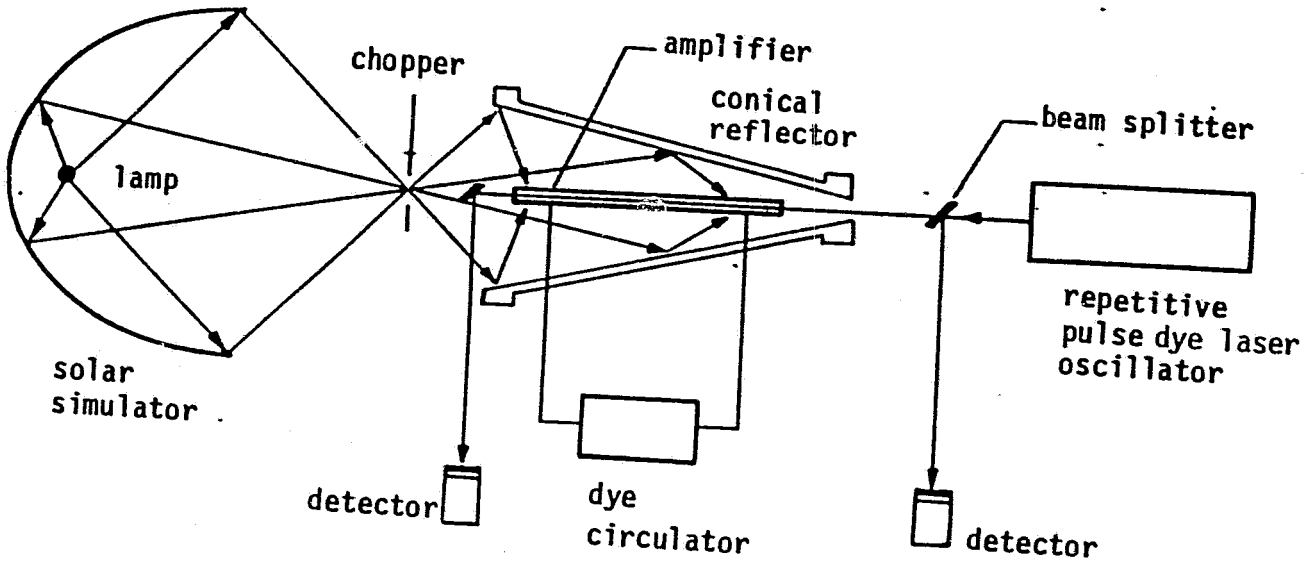

Fig. 10. The schematics of experimental setup for CW solar-pumped dye laser amplifier.

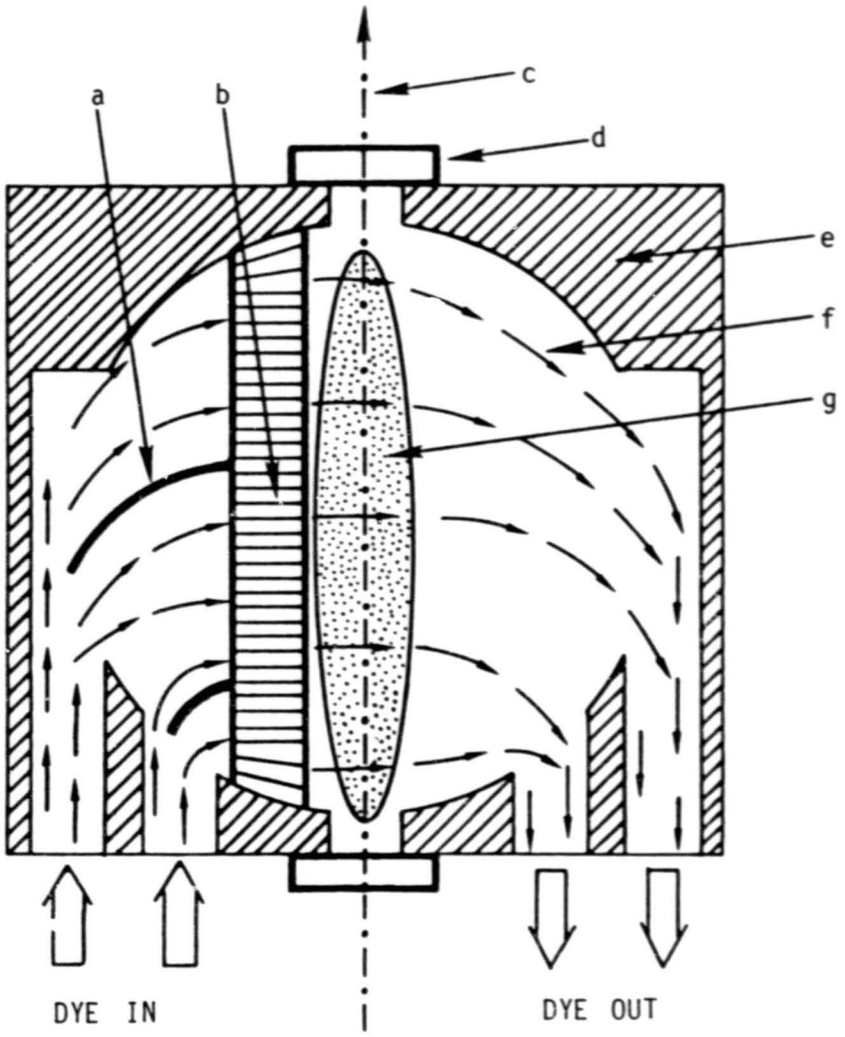

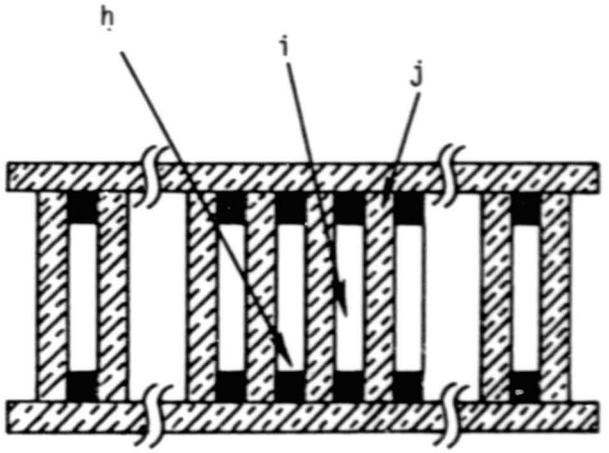

a - Diffraction plate
b - Straightner
c - Optical axis
d - window
e - Teflon body
f - Dye flow
g - Exposed region
h - Dye flow path
i - SS spacer (0.15mm)
j - SS plate (0.12mm)

Fig. 11 A cross sectional view of dye laser amplifier head and side view of straightner structure.

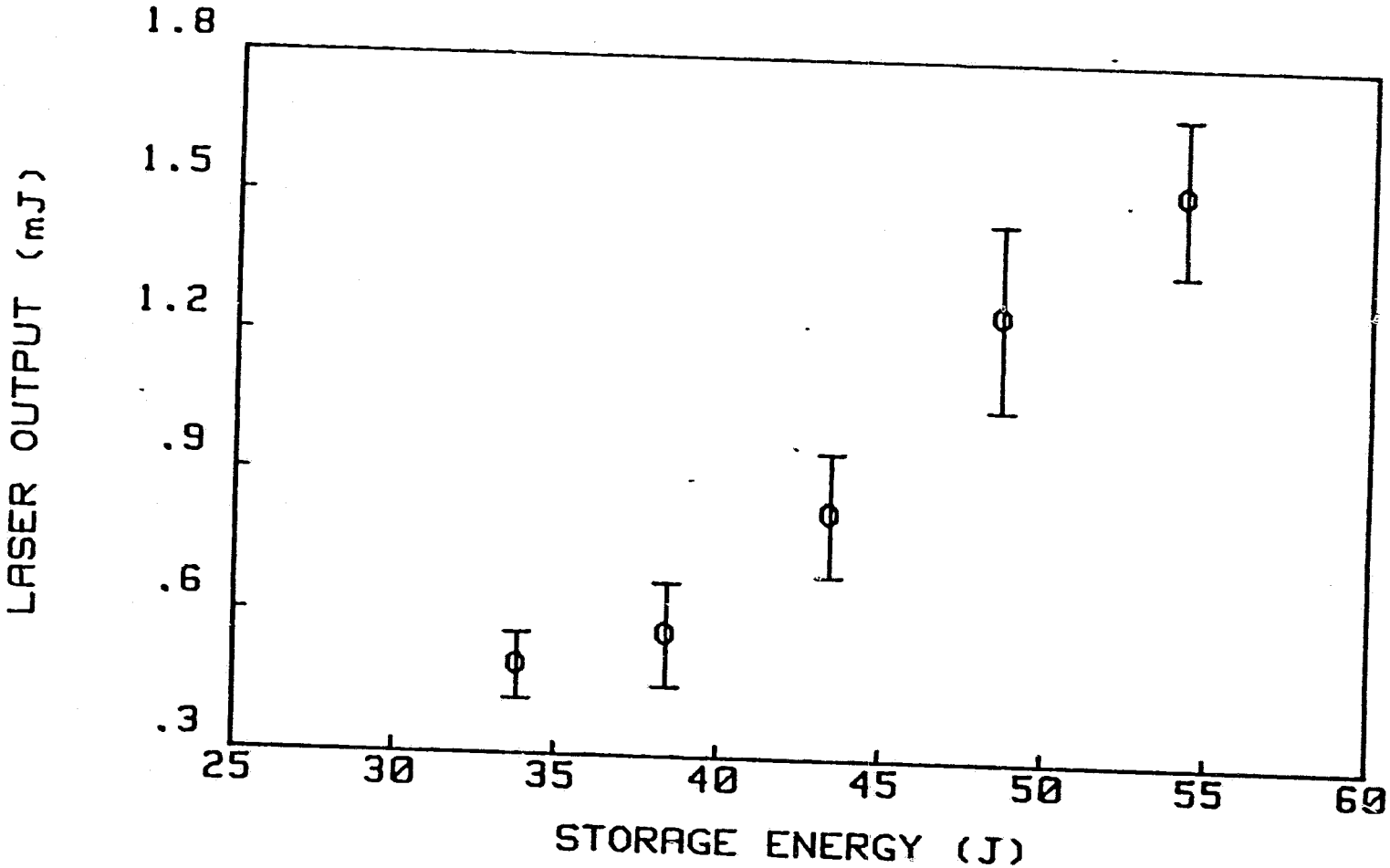

Fig. 12. The dye oscillator output as a function of input power.

Appendix

A MODEL FOR THE KINETICS OF A SOLAR-PUMPED* LONG PATH LASER EXPERIMENT*

Larry V. Stock - Hampton University

John W. Wilson and Russeel J. De Young - NASA Langley Research Center

Kwang S. Han - Hampton University

*To be published in NASA TECHNICAL PAPER

TABLE OF CONTENTS

Introduction 1

Solar Simulator Setup 2

Photolysis of the Alkyl Iodides 3

Results 10

Concluding Remarks 13

Table I 15

Table II 16

Table III 17

References 18

Figures 19

Abstract

A kinetic model for a solar simulator pumped iodine laser system is being developed and compared to an experiment in which the solar simulator output is dispersed over a large active volume (150 cm^3) with low simulator light intensity (= 200 solar constants). A trace foreign gas which quenches the upper level is introduced into the model. Furthermore, a constant representing optical absorption of the simulator emission is introduced, in addition to a constant representing the scattering at each of the mirrors, via the optical cavity time constant. The non-uniform heating of the gas is treated as well as the pressure change as a function of time within the cavity. With these new phenomena introduced into the kinetic model, a best reasonable fit to the experimental data is found by adjusting the reaction rate coefficients within the range of known uncertainity by numerical methods. The experimental parameters modeled are the lasing time, laser pulse energy, and the laser threshold.

INTRODUCTION

A model of a solar simulator pumped iodine laser is being developed. Previously, the simulator experiments were marked by a high solar concentration (≈10,000 suns) and a small volume (3 - 4 cm^3) excitation (ref. 1 and 2). In those studies it was shown that the laser threshold was dominated by the loss of the upper laser level through recombination and quenching (ref. 2). After threshold is achieved, since I_2 is a strong quencher of the upper laser level, the formation of I_2 is the dominate reaction which determines how long the system will lase. Because of the high solar concentration of prior experiments, I_2 buildup rate was sufficiently rapid that the laser was effectively quenched after about three milliseconds (ref. 1).

A new experimental system is presented here in which the solar simulator output is dispersed over a larger active volume (150 cm^3) and a greatly reduced simulator light intensity (≈200 suns) is used. With this new experimental design, the model is tested under vastly different operating conditions. Herein, information about the kinetic characteristics not accessible in earlier experiments is revealed. With the new experimental design, some changes are introduced into the model. A trace foreign gas which quenches the upper level is introduced into the system upon filling. A constant representing optical absorption is introduced via the optical cavity time constant (ref. 1). The non-uniform heating of the gas is treated as well as the pressure change as a function of time within the cavity. With these new phenomena introduced into the kinetic model, a best reasonable fit to the experimental data is found by adjusting the reaction rate coefficients within the range of known uncertainty by numerical methods.

SOLAR SIMULATOR SETUP

The present experimental setup has two light sources consisting of arc discharges across 8-mm gaps stabilized by a 1030-kPa (10.2 atm) Xe-flow. The light of the arc lamps is reflected from high quality elliptic aluminum reflectors and focused in shutter planes as shown in figure 1. The reflectors have a vapor deposited MgF_2 coating to prevent surface oxydation and abrasion. The spectral content of the arc plasma corresponds to black body emmission at 6000 K at the focus of each reflector. The divergent light beam leaving each focus is adjusted to intersect a flat plate collector cell in which the lasing gas is contained. The transparent cell walls are constructed of 6-mm thick UV enhanced fused silica plates.

The light intensity in the volume of excitation was measured with a calorimeter and the integral of the light intensity over the optical center line of the resonator cavity was calculated for each of the two lamps. Since the light intensity is relatively uniform in the volume of the resonator cavity, we assume a constant photodissociation rate averaged over the optical center line within the gas filled laser cell. The average solar concentration at the laser cell center line was found to be 150 suns over a 61.5 cm pathlength for the simulators operating at 400 amps each. The photodissociation rate is given by the average over the photodissociation cross section and results in (ref. 1 and 2)

$$\xi(\vec{x}) = T_t \, S \, n \, [f \exp(-n\sigma_0 x) + (1-f) \exp(-.223 n\sigma_0 x)] \, C(\vec{x}) \qquad (1)$$

where S (maximum photodissociation rate) and f (the fractional absorption near the line center) are given in table I. $C(\vec{x})$ is the local light

intensity in units of solar constants. The transmission coefficient for the 6-mm fused silica plates T_t is on the order of 0.96 and x is the slant distance through the gas in reaching the point $\vec{x}$.

PHOTOLYSIS OF THE ALKYL IODIDES

The chemical and physical processes of illumination of the alkyl iodides has been discussed elsewhere (ref. 1, 2, and 3). The major kinetic pathways due to photodissociation of alkyl iodide are shown in figure 2. It has been shown in previous studies (ref. 1 and 2) that laser threshold was dominated by the processes

$$R + I^* \rightarrow RI$$

which limits the amount of inversion achievable for a given light intensity, and

$$I^* + RI \rightarrow I + RI$$

which reduces the inversion intensity by loss of the upper level (ref. 2). As the kinetics of the system continues, there is a slow build up of I_2 which is a strong quencher of the upper laser level. The formation of I_2 is in competition with

$$R + I \rightarrow RI$$

and occurs through

$$I + I + RI \rightarrow I_2 + RI$$

which is a three body recombination reaction.

A model of the photodissociation and subsequent chemical reactions have been derived previously (ref. 1, 2, and 3) and are now given as

$$\frac{d[RI]}{dt} = K_1 [R] [I^*] + K_2 [R] [I] - \xi_1[RI] - K_4[R] [RI] \tag{2}$$

$$\frac{d[R]}{dt} = \xi_1 [RI] - K_1[R] [I^*] - K_2[R][I] - 2K_3[R]^2 - K_4 [R][RI] \tag{3}$$

$$\frac{d[R_2]}{dt} = K_3[R]^2 + K_4 [R][RI] \tag{4}$$

$$\frac{d[I_2]}{dt} = C_1 [I] [I^*] [RI] + C_2 [I]^2[RI] + C_3[I][I^*][I_2] + C_4[I]^2[I_2] - \xi_2[I_2] \tag{5}$$

$$\frac{d[I^*]}{dt} = \xi_1[RI] + \xi_2[I_2] - K_1[R][I^*] - C_1[I][I^*][RI] - C_3[I][I^*][I_2] - Q_1[I^*][RI] - Q_2[I^*][I_2] - r_{max} - A[I^*] - \frac{[I^*]}{\tau_D} - Q_{FG}[FG][I^*] \tag{6}$$

$$\frac{d[I]}{dt} = \xi_2[I_2] + Q_1[I^*][RI] + Q_2[I^*][I_2] - r_{max} - A[I^*] - C_1[I][I^*][RI] - 2C_2[I]^2 [RI] - C_3[I][I^*][I_2] - 2C_4[I]^2[I_2] - K_2[R][I] - \frac{[I]}{\tau_D} + Q_{FG}[FG][I^*] + K_4 [R][RI] \tag{7}$$

where [FG] is the foreign gas density and

$$\frac{d\rho}{dt} = r_{max} \frac{L}{L_C} - \frac{1}{\tau_C} \rho + gA[I^*] \quad (8)$$

$$r_{max} = c\sigma\rho ([I^*] - \frac{1}{2}[I]) \quad (9)$$

The kinetic rate coefficients for the propyl iodides were compiled elsewhere (ref. 2) with those results given in table II. The laser kinetics are discribed through equations (8) and (9) along with the corresponding coupling terms through the r_{max} variable of equations (6) and (7). The diffusion time constant may be evaluated from the point diffusion model as we did before (ref. 2) and show for a flat plate arrangement as we have here that

$$n_{I^*}(0,t) = n_0 \, erf(r_0/\sqrt{(4Dt)}) \quad (10)$$

It follows that the diffusion time constant is

$$\tau_D \approx 9 \, r_0^2/4D \quad (11)$$

where r_0 is the halfwidth of the laser cell and D is the diffusion constant.

$$D \approx 73 \text{ cm}^2 - \text{torr/sec} \quad (12)$$

as was found in reference 2.

Furthermore, because of the flat plate arrangement the optical cavity time constant τ_C is now given as

$$\tau_C = \frac{-2(L_C/c)}{\ln(r_1^7 r_2^4 r_3)} \quad (13)$$

where r_1 is the reflection coefficient (0.9975) at the corners of the cavity, r_2 is the Brewster window loss (.99), and r_3 is the output mirror reflectivity. The optical cavity time constant is modified as α_{loss} changes and is given as

$$\tau_c' = \frac{\tau_c}{(1 + c\alpha_{loss}\tau_c L/L_c)} \tag{14}$$

where α_{loss} is a parameter describing optical losses within the laser cavity. This parameter is found by including it in the parameter search along with the kinetic rate coefficients.

It is known that the main transition of the iodine laser is the 3-4 line. The gain on this line is

$$G_{34} = [\sum_{FF'} \sigma_{FF'}(\nu_{34})] \frac{g_3}{g_2 + g_3} \Delta I \tag{15}$$

where g_2, g_3 are the degeneracy of the hyperfine levels of the upper laser state, ν_{34} is the central frequency, and

$$\Delta I = [I^*] - \frac{1}{2}[I] \tag{16}$$

The individual stimulated emission cross sections $\sigma_{FF'}(\nu)$ are functions of the line broadening

$$\Delta\nu = \alpha_0 + \alpha_1 P_0 \tag{17}$$

where α_0 related to the Doppler linewith

$$\alpha_0 = 251 \sqrt{(T/T_0)} \quad (MHz) \tag{18}$$

and α_l is the pressure broadening coefficient taking on the value

$$\alpha_l = 14.8 \pm 4 \quad \text{(MHz/torr)} \tag{19}$$

at room temperature. The stimulated emission cross sections are then

$$\sigma_{FF'}(\nu) = \frac{\lambda^2 A_{FF'}}{8\pi} \, g_{FF'}(\nu) \tag{20}$$

where $g_{FF'}(\nu)$ is the corresponding line shape and $A_{FF'}$ is the transition rate. As a practical matter we take

$$\sigma_{34}^{*} = \frac{g_3}{g_2 + g_3} \sum_{FF'} \sigma_{FF'}(\nu_{23}) \tag{21}$$

as suggested by Fuss and Hola (ref. 4) for which

$$G_{34} = \sigma_{34}^{*} \Delta I \tag{22}$$

which is strictly true only when collisional equilibrium is established among the hyperfine levels.

An added complication of this experimental design is the long operation times of this laser system and the concern for overheating. Indeed, sufficient energy is deposited in the gas to raise the temperature by hundreds of degrees. Therefore, heat transport in the gas is of prime consideration. A simple model of heat diffusion from the volume of exposed gas to the cooler gas and the cell walls is now derived.

The heat diffusion equation is given as

$$k\Delta^2 T + q = \rho C \frac{dT}{dt} \tag{23}$$

where k is the thermal conductivity, q the source of heat from photolysis, and ρC the heat capacity per unit volume. Consider the steady state solution for constant heating in slab geometry with the initial gas temperature equal to the wall temperature T_w. The steady state gas temperature is given by

$$T(x) = \frac{1}{2} \frac{q}{k} (2r_0 - x)x + T_w \tag{24}$$

The study state heat flux at the walls is

$$q_0 = -k \left.\frac{dT}{dx}\right|_0 = qr_0 \tag{25a}$$

$$q_L = k \left.\frac{dT}{dx}\right|_{r_0} = qr_0 \tag{25b}$$

For which the total heat loss is

$$q_{tot} = 2qr_0 \tag{26}$$

for which an effective convection coefficient is found from

$$q_{tot} = h(T - T_w) = 2qr_0 \tag{27}$$

where T is the midpoint gas temperature

$$T = T_w + \frac{r_0^2}{2} \frac{q}{k} \tag{28}$$

for which h becomes

$$h = 4\, kr_0 \tag{29}$$

A two region model is assumed, as shown in figure 3. The temperature differential for the lasant medium directly exposed by the simulator light is given by

$$\frac{dT_1}{dt} = Q - (T_1 - T_w)/\tau_1 - (T_1 - T_2)/\tau_2 \tag{30}$$

and for the unexposed medium close to the wall

$$\frac{dT_2}{dt} = (T_1 - T_2)/\tau_2 - 1.5(T_2 - T_w)/\tau_1 \tag{31}$$

where τ_1 and τ_2 are relaxation times (~20 msec) for conduction to the wall and heat exchange between the two regions. The rate of internal heat generation of the system is approximated here as

$$Q = C_V \frac{\Delta E_{tot}\, T_w\ (°K)}{[RI]\ \ T_w\ (eV)} \tag{32}$$

where the specific heat at constant volume is approximated by $C_V = 3/2\ R$. The change in internal energy is given by

$$\Delta E = \varepsilon S_1 dt + \varepsilon_1 K_1 [I^*][R]\ dt + \varepsilon_2 K_2 [I][R]\ dt + \varepsilon_3 K_3 [R][R]\ dt \tag{33}$$

where ε_i is the energy released to the medium for the respective reactions (ref. 2).

The temperature change is related to the change in internal energy of the lasant's cavity and results in a fractional reduction in density in the heated region by $\rho(t)/\rho_o$, where ρ_o is the initial density and $\rho(t)$ is a function of time. Initially, the total volume of the cavity can be given as

$$V_t = V_o + V + V_i \tag{34}$$

where V_i, V_o and V are the regions interior, exterior, and directly influenced by the pulse energy (fig. 3). The pressures and temperatures of the regions interior and exterior to the laser pulse are assumed to be identical to the exposed region. Therefore, by use of conservation of energy, the effective temperature of the cavity is given as

$$T_{eff} = \frac{V}{V_{tot}} T_1 + \frac{V_o + V_i}{V_{tot}} T_2 \tag{35}$$

such that

$$V_i' = V_i \, P_o/P_{eff} \tag{36}$$

where the prime indicates the effective expanded volume and P_o the initial pressure. From this definition the fractional change in volume is given as

$$\frac{V'}{V} = 1 + \frac{V_o - V_i}{V} \left(1 - \frac{P_o}{P_{eff}}\right) \tag{37}$$

which becomes after the use of equations (35) and (36)

$$\rho(t) = \frac{\rho_o \, V/(V_o+V_i)}{V/(V_o+V_i) + [(1-T_1/T_2)/(1+T_1/T_2)]} \tag{38}$$

and this relationship is used to describe the change in pressure as a function of lasing time.

RESULTS

To develop the model further, a reasonable fit to the data must be found via an adjustment of the rate coefficients, the foreign gas partial pressure introduced into the system, and the change in the optical cavity

time constant describes the loss due to the optical absorption along the laser path. This is done by varying (ref. 5) these unknown parameters until a reasonable best fit to the experimental data is found for different fill pressures and output mirror reflectivities. This search is done while keeping in mind the constraints of the error bounds defined in table II for the rate coefficients, along with a best definition of what a reasonable fit to the experimental data may be. The results of the search are given in table III and, in addition, the foreign gas density [FG] is found to be 0.147×10^{13} cm^{-3} and in the optical cavity time constant τ_c

$$\alpha_{loss} = 0.82765 \times 10^{-4} + (0.105 \times 10^{-6})\ P_o \qquad (39)$$

where P_o is the fill pressure. The parameters found from the search are used to indicate the fit and are shown in figures 4, 5, and 6.

The experimental results for the C_3F_7 box laser are compared to the theory's prediction in figures 4, 5, and 6. In figure 4 the lasing time is plotted as a function of pressure; at high pressures the agreement is better than at low pressures. This may indicate that it is necessary for further physical constructions be added to the model. On the other hand, in figure 5 which shows the experimental and theoretical results of the threshold, except at low pressure there is good agreement with the experimental data. This is the result of the addition of a large amount of loss due to arosols and other unknown mechanisms along the lasing path in the model. In figure 6 the pulse energy is given as a function of experimental lasing times vs pressure. The energy calculation continued for the duration of experimental lasing time and this is the pulse energy

shown in relation to the fill pressures. If a comparison is made with the experimental results general trends are expressed in the pulse energy calculations given here.

Specifically, since the inversion density depends mainly on the kinetic coefficients K_1 and Q_1 and the diffusion coefficients (ref. 2), the lasing threshold is primarily due to these coefficients. In addition, a term α_{loss} describing the losses in the optical path is added into the calculation which affects the threshold times for the different experimental laser configurations. In the following descriptions the pulse energies and lasing times are for the individual reactions.

K_2 $\quad R + I \rightarrow RI$

Increase the value of K_2 and a larger number of parent molecules are produced for photodissociation. Thereby, the lasing times and energy would decrease.

C_2 $\quad I + I + RI \rightarrow I_2 + RI$

Increase the value of C_2, and the number of I_2 molecules is increased This mechanism gives shorter lasing times and less energy output since I_2 is a major quencher. In addition, fewer iodine atoms are available for recombination to the parent molecule RI.

K_1 $\quad I^* + R \rightarrow RI$

If K_1 is increased there are fewer excited iodine atoms to contribute to the pulse energy, thereby, reducing the power output and as stated above increasing threshold times.

Q_1 $\quad I^* + RI \rightarrow RI + I$

If Q_1 is increased the lasing times and pulse energies are reduced and the time to threshold is increased. This is because there are fewer excited iodine atoms.

$$Q_2 \quad I^* + I_2 \rightarrow I + I_2$$

If Q_2 is increased the lasing time is shortened since the population density of the metastable state is reduced. Furthermore, Q_2 is taken as the reaction rate for the unknown filling gas, further reducing the population density.

The remaining reactions are of lesser importance in the kinetic model. By increasing the value of K_3 in the model there are fewer radicals to recombine to form the parent gas RI. Therfore, the energy output is decreased. I_2 is a major quencher, therfore, if C_1 and C_3 are increased, energy outputs and lasing times decrease. The reactions governed by K_4 and C_4 do not affect the reaction until late laser times; later times than presently considered.

CONCLUDING REMARKS

As discussed earlier a best fit to the experimental data is found for the computer model as given here. Within the context of the best fit, the upper and lower constraints of the experimentally found values of the rate constants are maintained. The rate constants given in table III are used to calculate the results shown in figures 4, 5, and 6 for the lasing times,

threshold times, and pulse energy which represent a best reasonable fit. It is seen that trends are followed for the pulse energy and lasing times if experimental data for different fill pressures and output mirror reflectivities is compared to the model's predictions. Furthermore, except at low pressures there is good agreement with the threshold times given by the model. These disagreements at low pressures with the times to threshold and the lasing times suggests a further physical mechanism is necessary to be added to the model; perhaps a convection mechanism.

The introduction of the term for the filling gas suggests that there is an intrinsic amount of impurities in the system. In this case it is assumed the gas is inert. In addition, there is a further loss mechanism introduced as α_{loss}. In the model this parameter takes into account the losses introduced by arosol formation and other reproducible losses in the optical path. After the introduction of these mechanisms into the model, we find the rate coefficients by fitting to the experimental data, and these parameters represent a lower bound. Generally, since the trends are followed by the theoretical model as shown in figures 4, 5, and 6, the rate coefficients given in table III represent a best value when constrained to be within the range of known uncertainties (ref. 3). This means that except for K_4 and C_4 which would be significant at later lasing times than that considered here a best reasonable estimate for the rate coefficients is found.

Table I.- Photoabsorption Parameters Used for the Equivalent Power of One Solar Constant Exposure, 1.4 kW/m^2

Parameter	$n\text{-}C_3F_7I$	$i\text{-}C_3F_7I$	I_2 (ref. 7)
σ, cm^2	7.9×10^{-19}	6.2×10^{-19}	9.14×10^{-19}
λ_0, nm	272	275	499
δ_0, nm	12.7	14.5	23.0
Φ_I^*	1.0	1.0	0.51
S, sec^{-1}	3.04×10^{-3}	3.37×10^{-3}	3.38×10^{-2}
R_{λ_0}/R_{vis}	0.8	0.8	1.0
f	0.652	0.653	0.673

Table II. - Mean Reaction Rate Coefficients and Associated Uncertainty Factors Based on Literature Values

[The factor in parentheses gives the uncertainty limits associated with the coefficient]

Reactants	Products	Reaction rate coefficient, $(cm^3)^n/sec$		
		Symbol	R = $n\text{-}C_3F_7$	R = $i\text{-}C_3F_7$
R + R	R_2	K_3	$2.6 \times 10^{-12}(4)^{\pm 1}$	$9.0 \times 10^{-13}(3.8)^{\pm 1}$
R + I	RI	K_2	$2.3 \times 10^{-11}(3.5)^{\pm 1}$	$3.9 \times 10^{-11}(4.3)^{\pm 1}$
I + I + RI	I_2 + R	C_2	$8.5 \times 10^{-32}(5.3)^{\pm 1}$	$8.3 \times 10^{-32}(5.3)^{\pm 1}$
I + I + I_2	I_2 + I_2	C_4	$3.8 \times 10^{-30}(1.3)^{\pm 1}$	$3.8 \times 10^{-30}(1.3)^{\pm 1}$
R + RI	R_2 + I	K_4	3×10^{-16}	3×10^{-16}
R + I^*	RI	K_1	$5.6 \times 10^{-13}(6.2)^{\pm 1}$	$1.7 \times 10^{-13}(17)^{\pm 1}$
I^* + RI	I + RI	Q_1	$2.0 \times 10^{-16}(4.2)^{\pm 1}$	$7 \times 10^{-17}(4.1)^{\pm 1}$
I^* + I_2	I + I_2	Q_2	$1.9 \times 10^{-11}(2.6)^{\pm 1}$	$1.9 \times 10^{-11}(2.6)^{\pm 1}$
I^* + I + RI	I_2 + RI	C_1	$3.2 \times 10^{-33}(3.2)^{\pm 1}$	$3.2 \times 10^{-33}(3.2)^{\pm 1}$
I^* + I + I_2	I_2 + I_2	C_3	$8 \times 10^{-32}(1.8)^{\pm 1}$	$8 \times 10^{-32}(1.8)^{\pm 1}$
R + RI	R_2 + I^*	K_5	$3.2 \times 10^{-17}(3.2)^{\pm 1}$	$3.2 \times 10^{17}(3.2)^{\pm 1}$
I^* + RI	RI_2^*	K_6	$8.3 \times 10^{-18}(1.3)^{\pm 1}$	$6.5 \times 10^{-18}(1.1)^{\pm 1}$

Table III.- Reaction Rate Coefficients Found by Numerical Methods and Used in Laser Model.

Reaction rate coefficient, $(cm^3)^n/sec$	
Symbol	R = i-C_3F_7
K_3	9.0×10^{-13}
K_2	$3.9 \times 10^{-11}(4.3)$
C_2	$8.3 \times 10^{-32}\ (5.3)^{-1}$
C_4	3.8×10^{-30}
K_4	3×10^{-16}
K_1	$1.7 \times 10^{-13}\ (17)$
Q_1	$7.0 \times 10^{-17}\ (4.1)^{-0.72}$
Q_2	$1.9 \times 10^{-11}\ (2.6)^{-1.0}$
C_1	$3.2 \times 10^{-33}\ (3.2)^{-0.93}$
C_3	8.0×10^{-32}

REFERENCES

1. Wilson, J.W.; Raju, S.; and Shiu, Y.J.: Solar-Simulator-Pumped Atomic Iodine Laser Kinetics. NASA TP-2182, August 1983.

2. Wilson, J.W.; Lee, Y.; Weaver, W.R.; Humes, D.H.; and Lee J.H.: Threshold Kinetics of a Solar-Simulator-Pumped Iodine Laser. NASA TP-2241 February 1984.

3. Brederlow, G.; Fill, E.; and Witte, K.J.: The High-Power Iodine Laser Springer-Verlag, Berlin 1983.

4. Fuss, W.; and Hohla, K. (D.K. Dreyer and R.E. Reverly III, transl.): Pressure Broadening of the 1.3 μm Iodine Laser Line. Rep. No. IPP IV/67, Max-Plank-Inst. Fur Plasmaphysik (Garching Bei Munchen), Dec. 1974. Also Fuss, W.; and Hohla, K.: Pressure Broadening of the 1,3 μm Iodine Laser Line. Z. Naturforsch., vol. 31a, no. 6, June 1976, pp. 569-577.

5. Stock, L. V.; Wilson, J. W.; and Han, K. S.: Simulation Problem for Solar-Pumped Laser. Annual Meeting of Virginia Academy of Science, May 17, 1985.

FIGURES

1. Solar pumped long path laser experiment.

2. Iodine laser kinetics.

3. Temperatures and volumes used to model pressure changes within the active region of the laser cavity.

4. Results of kinetic model using rate coefficients given in table III for lasing times vs pressure for 85 percent and 97 percent reflectivities as compared to experimental data.

5. Results of kinetic model using rate coefficients given in table III for threshold times vs pressure for 85 percent and 97 percent reflectivities as compared to experimental data.

6. Results of kinetic mode using rate coefficients given in table III and cut-off times given by experiment for pulse energy vs pressure for 85 percent and 97 percent reflectivities as compared to experimental data.

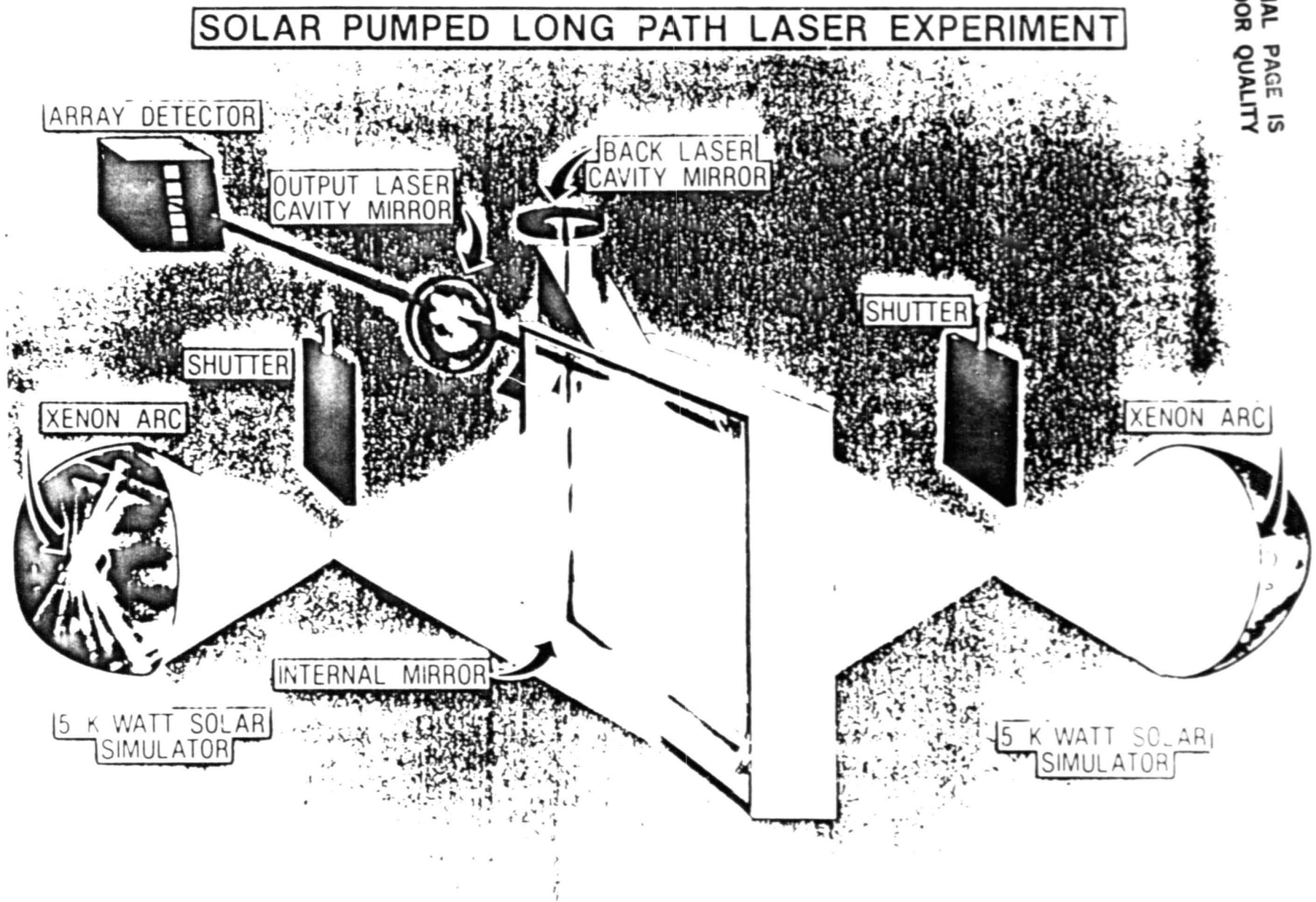

Fig. 1. Solar pumped long path laser experiment.

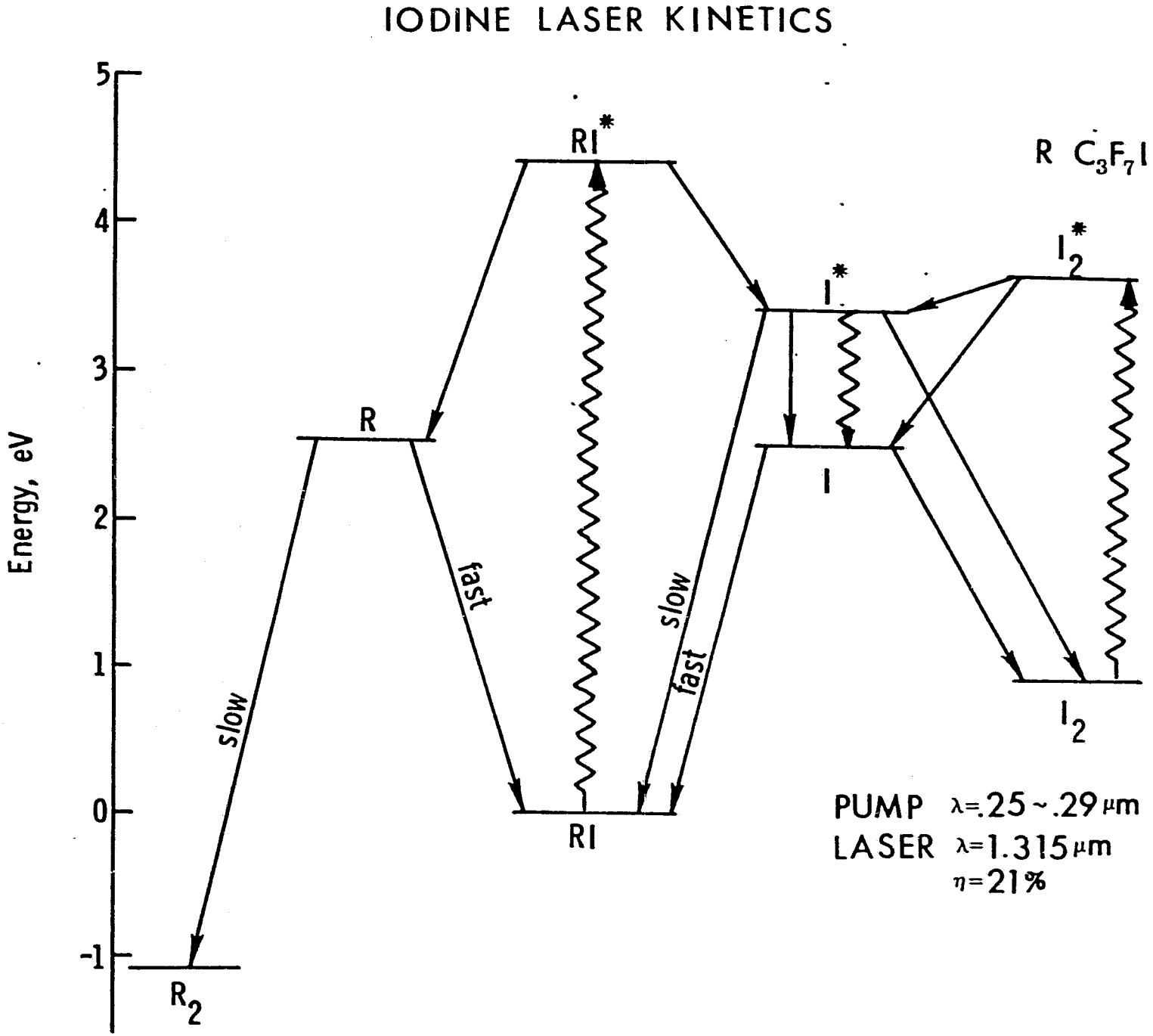

Fig. 2. Iodine laser kinetics.

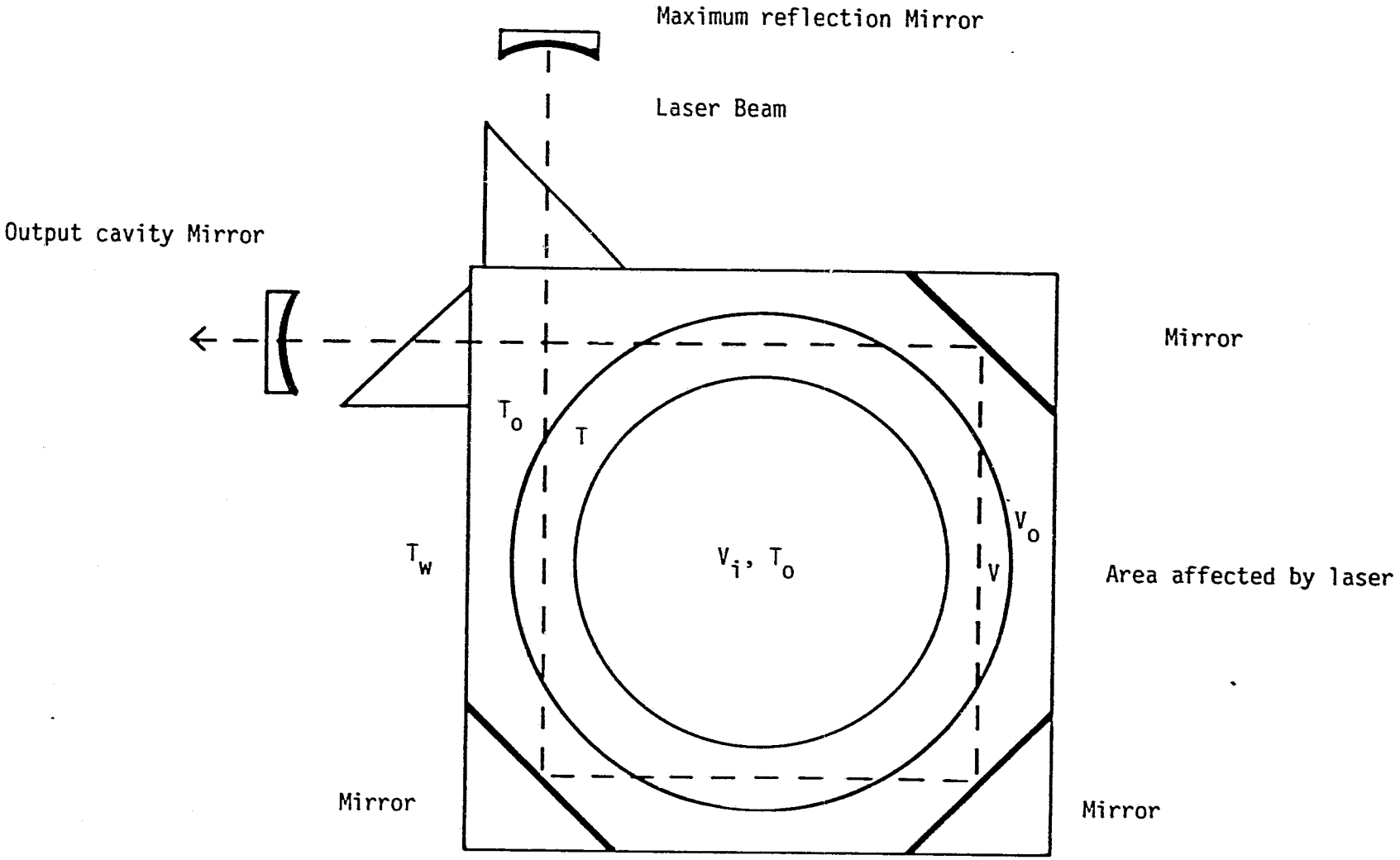

Fig. 3 Temperatures and volumes used to model pressure change within the active region of the laser cavity.

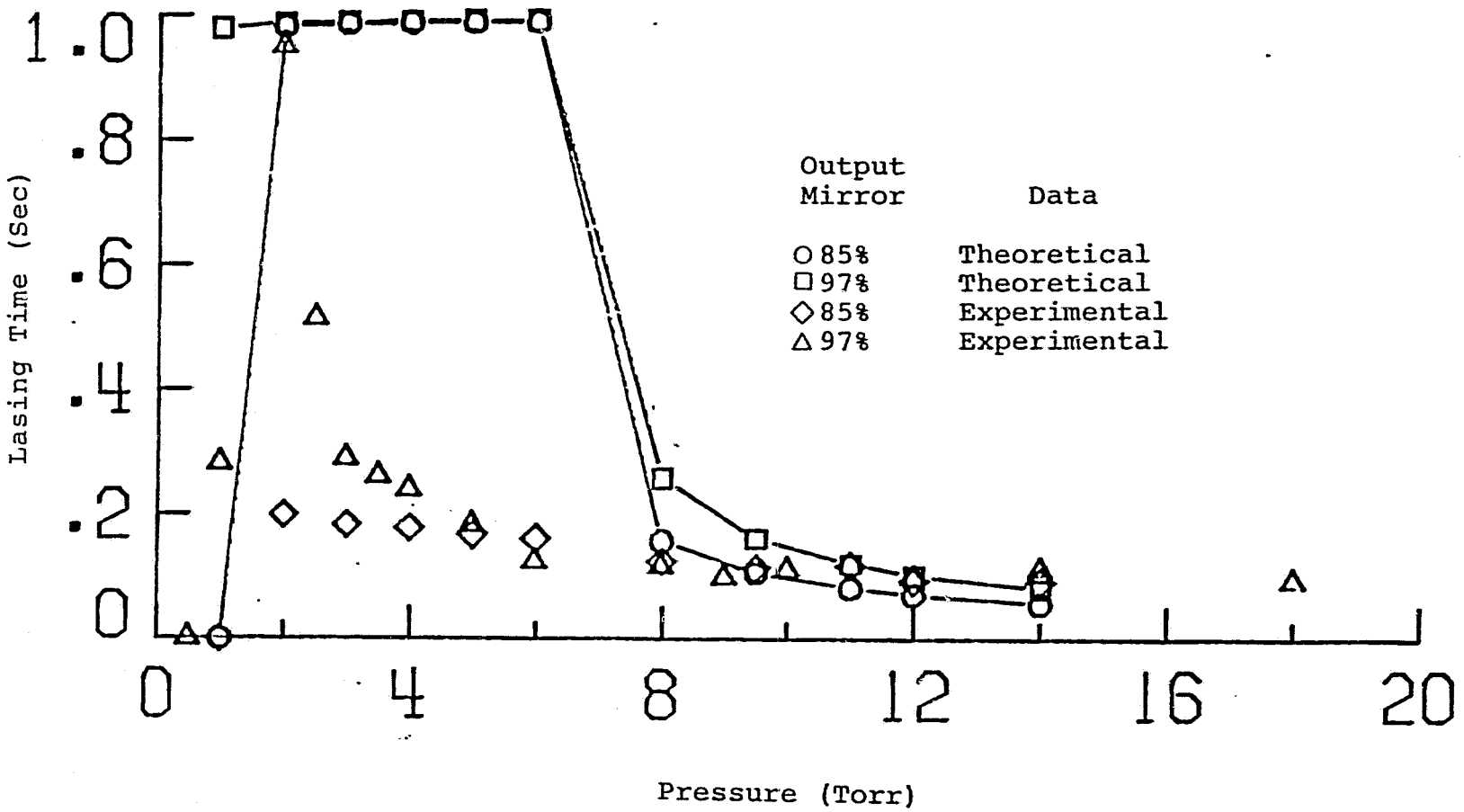

Fig. 4. Results of kinetic model using rate coefficients given in table III for lasing times vs pressure for 85 percent and 97 percent reflectivities as compared to experimental data.

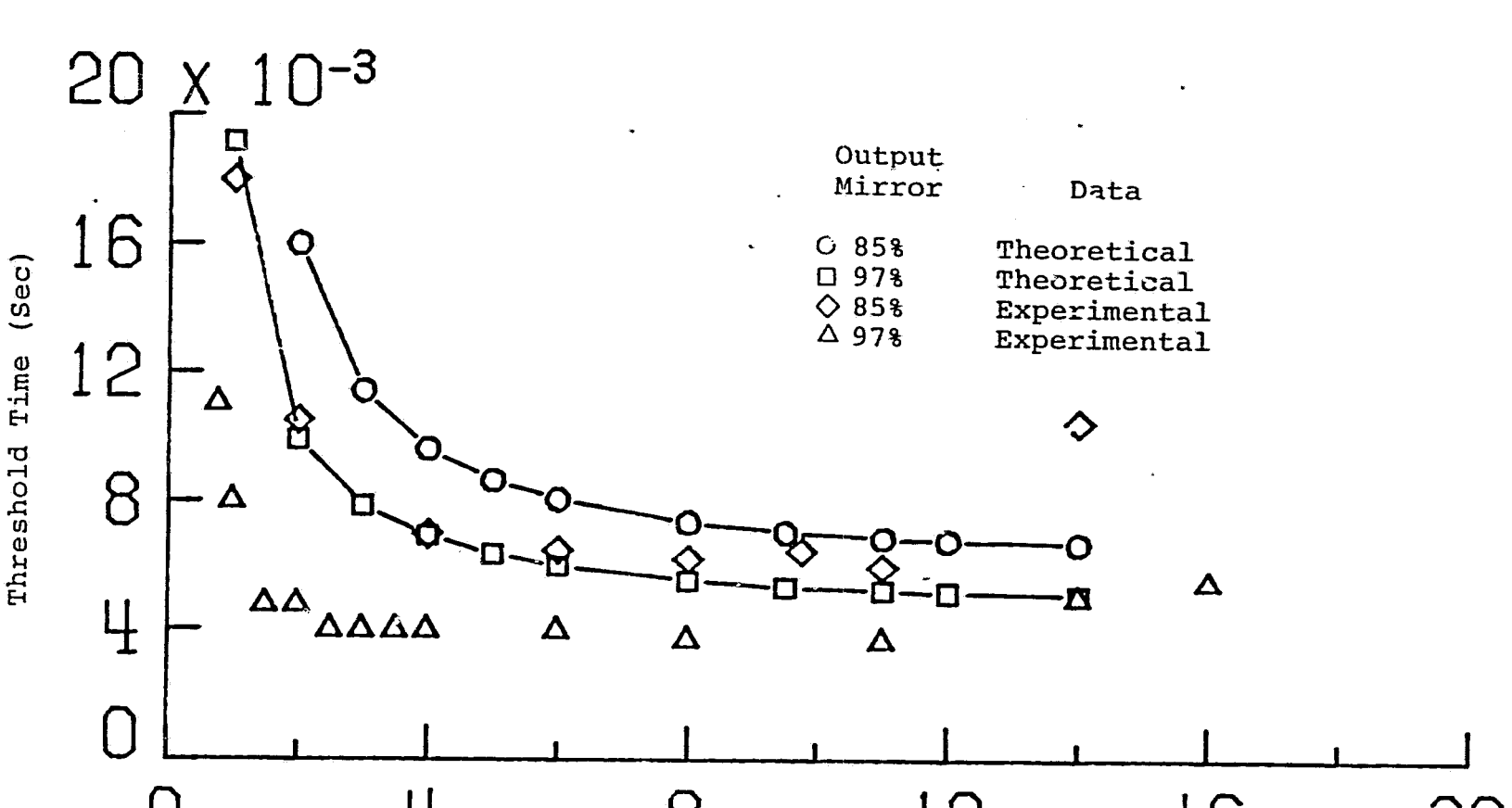

Fig. 5. Results of kinetic model using rate coefficients given in table III for threshold times vs pressure for 85 percent and 97 percent reflectivities as compared to experimental data.

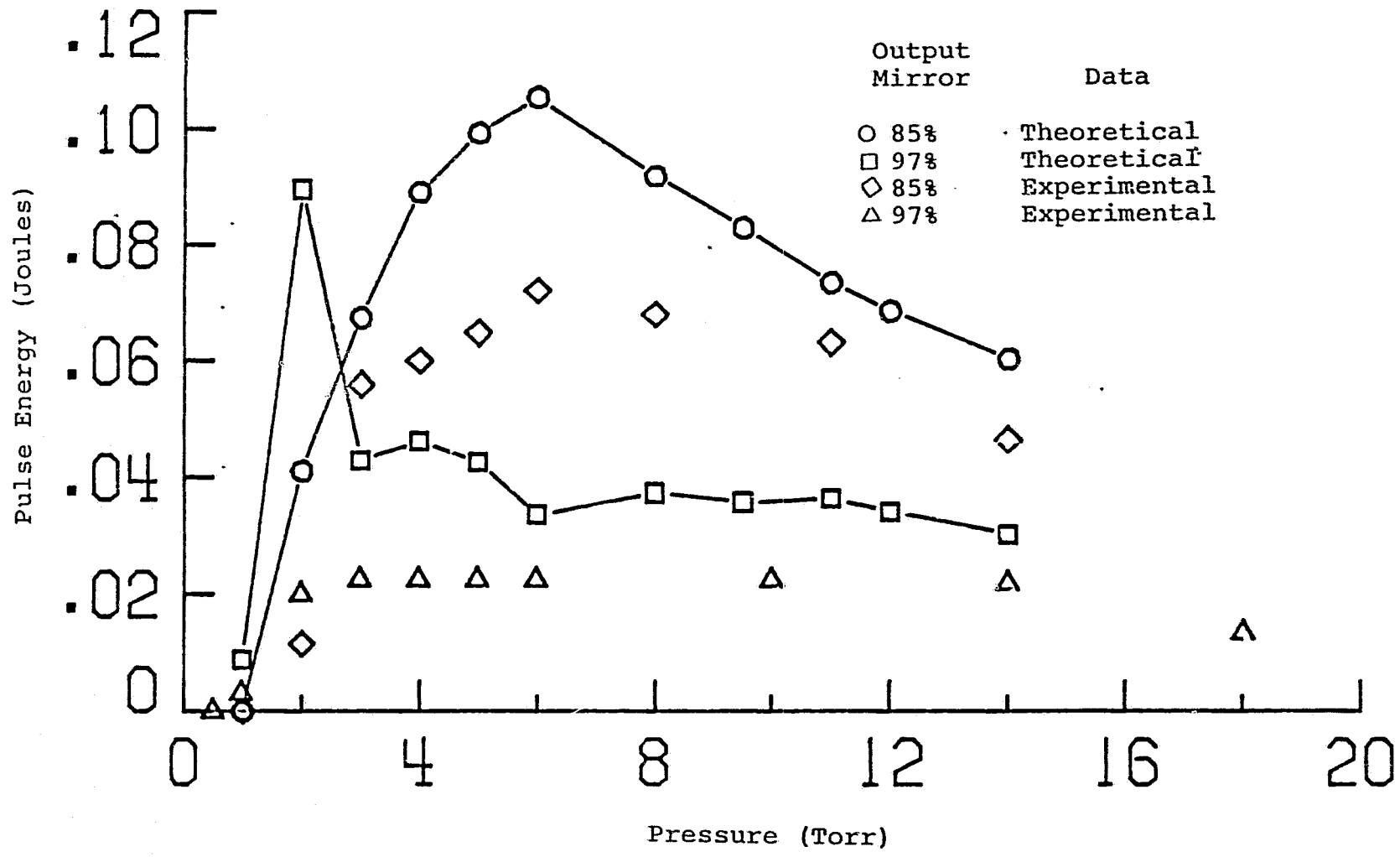

Fig. 6. Results of kinetic model using rate coefficients given in table III and cut-off times given by experiment for pulse energy vs pressure for 85 percent and 97 percent reflectivities as compared to experimental data.